ELSEVIER

Polymer 42 (2001) 4675–4685

polymer

www.elsevier.nl/locate/polymer

Spherulitic banding in metallocene catalysed polyethylene spherulites

J.J. Janimak*, L. Markey, G.C. Stevens

Polymer Research Centre, School of Physics and Chemistry, University of Surrey, Guildford Surrey GU2 7XH, UK

Received 14 April 2000; received in revised form 10 August 2000; accepted 22 August 2000

Abstract

Atomic force microscopy (AFM) and transmission electron microscopy (TEM) have been used to examine the influence of molecular weight on the melt-crystallised morphology of a series of permanganically etched metallocene catalysed high-density polyethylenes (mHDPEs). The effect of increasing molecular weight is manifest by different morphologies, viz. banded spherulites and lamellar domains structures above a critical molecular weight, and sheaf-like structures below a critical molecular weight. In addition, the incipient spherulite development has been detected in a low molecular weight mHDPE. AFM height imaging of permanganically etched sections has revealed an apparent band period spacing decreasing from the centre of any given spherulite in non-diametral sections of isothermally crystallised samples. This observation was also confirmed by exhaustive TEM measurements on similar non-diametral sections. AFM height measurements show that band height amplitude varies across bands as a function of radial position and is a characteristic feature of all the banded spherulitc structures studied. The band amplitude and period are dependent on molecular weight and are sensitive to the degree of etching with fast etching rates for low molecular weight mHDPEs. Both the AFM and TEM measurements of the apparent band spacing converge with radial distance to the true band period spacing. Homopolymers and copolymers show a different relationship of true band spacing with molecular weight.

Keywords: Polymer spherulites; Spherulitic banding; Polyethylene spherulites

1. Introduction

Polymer spherulites are an important morphological form in semicrystalline polymers frequently observed between the cross-polars of an optical microscope [1–7]. Historically, spherulites have been the subject of much research, dating as far back as the late nineteenth century when low molecular weight organic and inorganic materials were discovered exhibiting spherulitic structure [8]. Spherulites are characterised by their radial growth pattern that evolves into spherical symmetry [9]. The essential ingredients of spherulitic crystallisation are much the same for a diverse number of materials, many of which are inorganic [10–12]. Banded spherulites on the other hand have been unambiguously identified as exhibiting a regular arrangement of birefringent units along the spherulite radius [1–7,13]. Under isothermal crystallisation conditions, the appearance of a constant helical pattern is inferred from conventional optical and electron microscopies without any direct measure of band profile. These observations have led to universal acceptance of a regular band period spacing. In other words every one half twist (π-rotation about the spherulite radius) corresponds to one band period spacing. However, the origin and observation of a banded spherulite is largely determined by choice of catalyst, molecular weight of the polymer and an appropriate nucleation and crystallisation process, anyone of which may produce a dominant effect. In a previous study of medium density polyethylenes, we have found a wide range of resulting morphologies extending from lamellae domaining through to fully developed banded spherulites whose band period is controlled by molecular characteristics and crystallisation conditions [14].

Spherulites are essentially spherical aggregates of anisotropic crystalline lamellae that emanate from a common central nucleus. For example, in a diametral section, **b** is always radial, while **c** is near normal to the page for flat-on lamellae and **a** for those seen edge-on. Conversely, **b** is normal to the page at the centre of a spherulite, similar to non-spherical aggregates that develop into sheaf-like objects. To illustrate this Fig. 1 shows a three-dimensional schematic representation of a spherulite during the early stages of growth. Sizes and types of nuclei may vary from one system to the next and in the case of polyethylene, this may range from a few nanometers and from heterogeneous to homogeneous nucleation but on the whole nucleation is not well understood in polyethylene. The appearance of an

* Corresponding author. Lilly Clinical Operations SA, Parc Scientifique de Louvain-la-Neuve, Rue Granbonpré 11, 1348 Mont-Saint-Guibert, Belgium.

0032-3861/01/$ - see front matter
PII: S0032-3861(00)00637-6

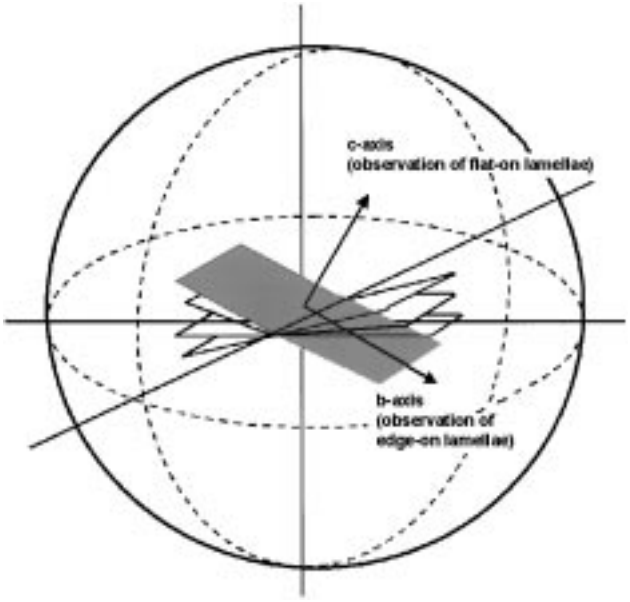

Fig. 1. An illustration of the interior of a spherulite nucleus showing different projections for edge-on and flat-on lamellae.

asymmetrical orientation of crystals and in the case of banded spherulites co-ordinated orientation give spherulites their principal characteristic [15]. In the past several years exceptionally large banded spherulites have been reported in a polymer blend containing maleic anhydride and 2 wt% polyacrylonitrile [16]. The spacing of the bands ranged from 4 to 15 mm, in some cases larger than the specimen thickness, making it possible to determine the exact molecular orientation from X-ray diffraction.

Until very recently, use of the atomic force microscope (AFM) to reveal the microstructure and lamellar organisation in semicrystalline polymers was undertaken by revisiting published investigations with conventional microscopies [17]. Fortunately, advances in probe microscopy have enabled real-time in-situ measurements under conditions of isothermal crystallisation. Using AFM the growth front velocities of several commercially important spherulitic systems have now been investigated [18–20]. These dynamic experiments using AFM tapping mode phase and height imaging have revealed 3D topographic profiles of surfaces with nanometer scale resolution providing further insight into the evolution of spherulites in particular and banded spherulites in general. Among the systems where banded structures have been studied, the biological thermoplastic poly(hydroxybutyrate) (PHB) and its copolymers with hydroxyvalerate (PHB/V) have yielded some of the most revealing results [18]. Interestingly in PHB, a depression in the height image was observed in front of the growing spherulite, indicating the large-scale motion in the non-crystalline phase due to volume contraction on crystallisation. The key advantage of using AFM over conventional Transmission Electron Microscopy (TEM) is its ability to image topographically polymer surfaces without the need for surface electron enrichment, circumventing the need to prepare time consuming two-stage carbon replicas [21]. An additional advantage of the AFM is the enhanced spatial and lateral resolution. By combining AFM with TEM in a complementary role, it has now become possible to examine in mesoscopic detail the structure of the growth front after cessation of crystallisation [18–20].

In this paper, we have pursued only the issue of banding and have focussed on estimating band period spacing and height amplitude from AFM height imaging following permanganic etching. A family of metallocene catalysed polyethylenes with different molecular weights and level of short chain branching was used for this purpose. In particular, the issue of helicoidal lamella twisting through the formation of a helical lamella orientation or a co-operative interleaving of curved lamellar stacks is discussed here [22,23]. By examining permanganically etched specimens we have attempted to differentiate these particular features of polymer morphology in polyethylenes and banded spherulites in particular. Lamellar curvature and lamellar twisting on banding are considered in parallel with polymer molecular weight distribution and where possible level of short chain branching. In view of the application of these materials, namely, packaging film, gas and water pipelines, etc. understanding the relationship between molecular organisation and microstructure is paramount. Metallocene catalysed polyethylenes are also perceived as being commercially significant and technically different from conventional heterogeneous systems in respect of their structure–property relationships [24–26]. The main difference between resins made from metallocene catalysts and those made with conventional Philips or Ziegler–Natta catalysts is that the former yields predominately a narrower molecular weight distribution. In addition, with metallocene copolymers the presence of short side-chains statistically positioned homogeneously along the molecular chains enables well-defined banded spherulites to be formed under a range of crystallisation conditions [27,28].

2. Materials and equipment

Our medium and high density polyethylenes with known branch content, molecular weight and polydispersity were kindly provided by Fina Research (Belgium) and Solvay (Belgium) through the Fina Surrey Scholar research programme. Molecular characteristics of as received materials are listed in Table 1.

2.1. Specimen preparation and electron microscopy

For examination in the electron microscope specimens were melt-crystallised under a dry nitrogen atmosphere at 170°C in a Linkam hot stage and subsequently cooled at 15°C/min down to room temperature. Samples were then microtomed at room temperature using a rotary microtome

Table 1
Molecular and melting characteristics of as received material. Short chain branch content was assessed using ^{13}C NMR

Reference Resin type	Units	Polymer A Homopolymer	Polymer B Homopolymer	Polymer C Homopolymer	Polymer D Copolymer	Polymer E Homopolymer	Polymer F Copolymer	Polymer G Copolymer
Density	g/cm^3	0.9602	0.970	0.9545	0.9508	0.9374	0.9418	0.9404
M_n	kda	23.4	8.4	30.8	27.3	86	8.7	31.4
M_w	kda	79	22	118	100.4	281	98	99.2
M_z	kda	246	52	321	305	629	360	226
M_w/M_n		3.38	2.62	3.83	3.68	3.27	11.26	3.16
SCB(/1000C)[a]		0	0	0	0.2	0	3.6	1.4
T_m	°C	133.9	133.6	131.8	134.1	136.7	123.8	129.8
ΔH_m[b]	J/g	220.4	251.2	217.1	212.9	199.2	203.3	192.5

[a] 1-Hexene comonomer.
[b] 100% Crystallinity (293 J/g).

removing successive slices of approximately 5 μm in thickness. An optical microscope with interference contrast was used periodically to assess the progress of microtoming. Specimens were etched for 3 h in an etchant consisting of a 1% w/v solution of potassium permanganate dissolved in 2:1 sulphuric and dry ortho-phosphoric acids [29]. Periodic checks on the progress of etching were undertaken, by arresting the etching process and observing development with the optical microscope. For TEM work, a standard two-stage indirect carbon replica was made of the etched specimen (using cellulose acetate film moistened with acetone). These replicas, which were several tens of nanometers in thickness, were then transferred to copper grids for examination in the transmission electron microscope. A Philips 400T electron microscope with EDS capability was used to examine carbon replicas in bright field mode under an accelerating voltage of 80 kV. Specimens were mounted in a rotating goniometer stage capable of *xy* movement in the plane of the specimen as well as in/out-of-plane tilt. Tilting of replicas with respect to the electron beam was used occasionally to enhance resolution and to obtain clarity of complicated microstructural details.

2.2. Scanning probe microscopy

Permanganically etched samples were observed directly using tapping mode AFM on a Digital Instrument Nanoscope III scanning probe microscope, using NT-MDT non-contact ultrasharp silicon cantilevers or DI 'nanosensors' tips. Experiments were conducted in the tapping mode with the cantilever vibrating near its resonance frequency. Topographic data was recorded, along with the phase signal (phase between the recorded cantilever oscillation signal and the piezo excitation of the cantilever) which gives additional information not available from the topographic study alone. Vertical cross-sections were taken from unmodified topographic images to reveal the surface profile of permanganically etched banded spherulites. Where specified, topographic data was processed for contrast enhancement using a standard DI programme which runs a statistical differencing filter that enhances the contrast of edge and line features, enabling to reveal lamellae structure. This image treatment distorts the *z*-axis scale. This accounts for why the *z*-axis height bar is not displayed next to the contrast-enhanced images. The phase images were also useful in providing features very similar to those observed in TEM. Special care and attention was given to identifying and eliminating artefacts arising from spurious tip/surface interactions.

3. Results and discussion

3.1. General polymer microstructure

Examination of permanganically etched melt-crystallised lamellar morphology of the high density metallocene catalysed polyethylenes (mHDPEs) shows a marked dependence on molecular weight. Fig. 2a–c (discussed later) illustrate examples of banded spherulites observed in TEM of permanganically-etched sections of melt-crystallised polymers A, C and D, respectively.

In the following, the apparent band spacing measurements from AFM and TEM images of non-diametral spherulite sections are differentiated from the true band spacing which would be obtained from diametral sections. The determination of the true band spacing from non-diametral section observations is discussed later in this paper.

Fig. 3 shows the true spherulite band spacings as measured from TEM and AFM on five materials, three copolymers of near identical molecular weight and two homopolymers of different molecular weight. This plot of band spacing against weight average molecular weight for both metallocene catalysed homopolymers and copolymers is interesting. The dashed line of negative slope through the two homopolymers would if produced eventually reach zero, which suggests that at higher molecular weight, the banding phenomenon will 'self-extinguish' for molecular reasons. The point of copolymer D lies very near the intersection of copolymer line and the homopolymer line. This is as would be expected, since polymer D in fact is of very low branch content, and also of similar polydispersity to the two homopolymers. The tighter banding in polymers F and G is most probably related to their higher

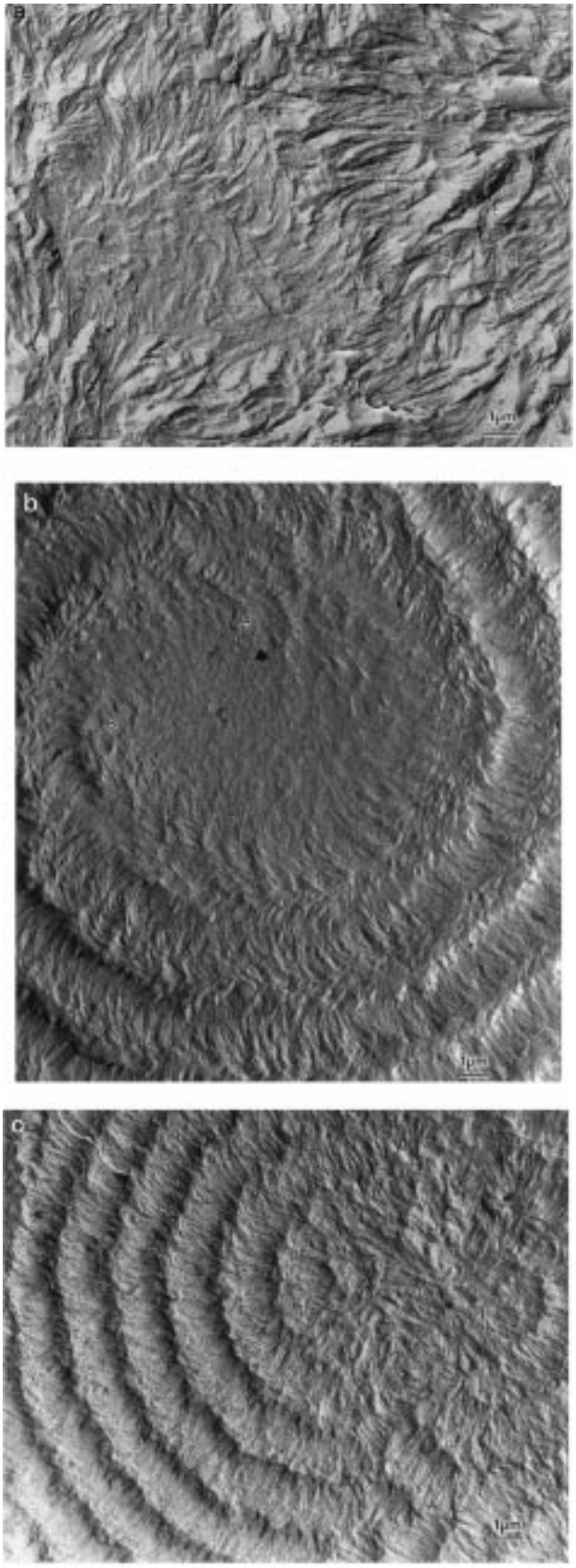

Fig. 2. Illustrated examples of banded spherulites observed in TEM of permanganically etched sections of polymers. (a) Polymer A showing several impinged immature spherulites and screw dislocations with dominant curved shaped lamellae. In-filling lamellae can be found when edge-on splay to a flat-on orientation. (b) Polymer C showing screw dislocations and dominant curved shaped lamellae with in-filling lying in-between dominant lamellae. (c) Polymer D a high density copolymer exhibiting a mature banded structure has demonstrated by the large number of bands present.

branch content, but the greater polydispersity of F may be acting in opposition to the branch content, since these two points are much closer together than if their spread were due to branch content alone.

In the case of homopolymer banded spherulites, the true band period spacing is observed to contract with increasing molecular weight. Since identical catalysts were used, we suspect that faster crystallisation rates allied to molecular segregation effects may be responsible for the observed behaviour. However, in the case of copolymers, an opposite trend is seen with increasing molecular weight, because a small disproportionate amount of short chain branching may increase the concentration of segregant species by reducing the overall size of spherulites and the true band spacing.

3.2. TEM–AFM comparisons

The typical microstructure of polymer B, our lowest molecular weight sample is illustrated in Fig. 4a. This incipient non-banded spherulite specimen possesses characteristics common to most spherulitic growth. Long parallel strips of closely packed lamellae can be seen extending radially, forming crenellated patterns (flower petal shapes) at the boundary between adjacent spherulites. The term incipient 'spherulite' used here describes the anisotropic immature form seen predominately in slow growing more densely nucleated semicrystalline polymers. In this state of complete crystallisation the overall relief is sheaf like in appearance, however, the occurrence of screw dislocations highlighted by arrows indicate features that are synonymous with more fully developed spherulites, namely lamellar small-angle branching and splaying. The observed stacked lamellar arrangement is not perfectly flat as one would initially expect because as highlighted in Fig. 4b and shown schematically in Fig. 4c, kinks or stacking faults can develop which create lamellar splaying. The kink represents a plane undergoing lamellar divergence. This lamellar divergence continues to persist radially coming to a halt short of the spherulite edge. In other words the area highlighted between points A and A′ is a good example of lamellar stacks in immature spherulites diverging within an open framework tens of microns in diameter. Lamellar divergence, which is thought to occur through rejection of cilia from adjacent lamellae, persists along the length of a lamella [15]. This mechanism is not exclusive to spherulitic geometries or banding in particular, it is generic to all folded-chain semicrystalline polymers.

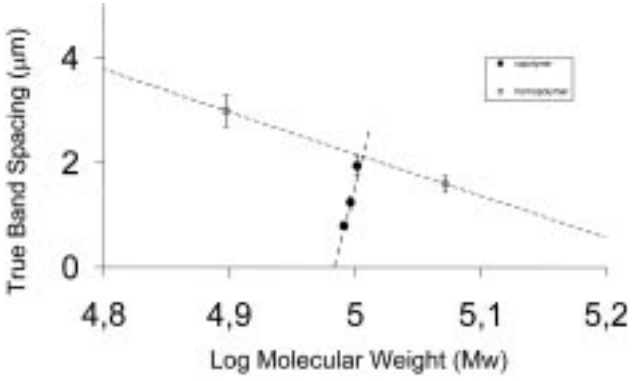

Fig. 3. A plot of average true band spacing as measured from TEM and AFM on five materials, three copolymers of near identical molecular weight and two homopolymers (polymer A and C) of different molecular weight. Scatter in the data is represented by error bars.

AFM contrast enhanced height images and phase images of polymer B are shown in Fig. 5a and b, respectively. Fig. 5a shows a general view (8 μm by 8 μm image) confirming the immature incipient spherulitic structure. Fig. 5b shows a higher magnification image (3 μm × 3 μm) of the same surface but in phase image mode. The height relief can be considered as an assessment of the roughness developed through etching, which for this particular sample achieved a maximum of 300 nm. Fig. 5a also reveals the large open lamellar structures seen earlier in Fig. 4a which when viewed in the phase image (see Fig. 5b) show greater lamellar contrast. Unoriented individual planar-profiled lamellae are seen emanating from beneath the underlying crystalline texture. By examining the features of one or two examples (shown here highlighted with arrows), of lamellae standing proud of the surface they appear to be curved but untwisted along their long axis. Earlier Bassett et al. applied chlorosulphonation techniques to banded spherulites (Marlex 5, Phillips Petroleum) and from their tilting experiments in the electron microscope they found that the molecular orientation of stained lamellae were curved and untwisted [30]. The origins and appearance of the twisted lamellar arrangement is thought possible by considering the average crystal orientation about **b**. A change in the relative orientation of essentially untwisted lamellae could account for banding in this way.

With increasing molecular weight the number of immature spherulites become denser, i.e. smaller size sheaves leading to well-defined inter-spherulitic interfaces. Fig. 2a of polymer A is representative of this type of morphology grown under slow cooled crystallisation conditions. Lamellae approximately similar in thickness to those shown in Fig. 4a ~250 Å are finely dispersed with evidence of smaller in-filling lamellae between dominant lamellar structure. Long curved lamellae, at least 2 μm in length form the essential skeletal framework which we believe is necessary to sustain the observed banding habit. The overall texture is one of impinging spherulites with the first significant signs that lamellae are organised within periodic banded structures. Even in their infancy with just a few bands, these banded spherulites bear all the characteristic traits of mature banded spherulites, namely curved lamellae and well-defined interspherulitic boundaries. From TEM, we have estimated an apparent band period spacing average of approximately 3 μm for this polymer. It is generally accepted that the propagation of single flat lamellae in three-dimensional growth occurs by screw dislocations, where one lamellae divides into two which then grow apart at a small angle. In this particular specimen, because banding is such a pervasive feature we actually see little evidence for this mechanism. Instead, screw dislocations that are in some way connected with banding must form regularly and with the same handedness ensuring that daughter lamellae formed on outward growth do so at a continually increasing angle. From these TEM images the development of the band structure and band periodicity is probably linked to an incremental process relying heavily on molecular weight, lamellar size and molecular co-operatively.

We discovered in an earlier study involving ethylene 1-hexene copolymers that the occurrence of banded spherulites is particularly sensitive to the type of catalyst used than to any other single molecular variable [14]. Materials with similar densities and molecular weight characteristics and level of short chain branching can have completely different morphologies. Fig. 6 shows contrast enhanced topographic AFM images of polymer A. Fig. 6a shows a large scan size (low magnification) and Fig. 6b a higher magnification image of the band structure. The low magnification view confirms many of the gross morphological features observed earlier in Fig. 2a, namely the presence of banding. In this particular molecular weight range, the characteristic features associated with banding are easily imaged. The various height images collected on this sample indicate that the vertical distance between the lowest and highest point on the sample surface (band height amplitude) ranged from 300 to 600 nm. This range is higher than in the previous sample, where crystallinity was significantly greater and lamellar thickness was marginally smaller. In Fig. 5a, the distinct steps in height contrast are exemplified by the alternating contrast change from light to dark and vice-versa. This modulation in contrast is aperiodic and produces an image similar to that seen in chlorosulphonic acid stained sections.

Fig. 2b shows the etched TEM melt-crystallised morphology of polymer C, an intermediate molecular weight material (118 k). Compared with polymer A, this material is replete with well-developed banded spherulites The crispness of this electron micrograph probably owns a great deal to the way in which the etching process has selectively removed the polymer material. This polymer in contrast to the previous samples has lower crystallinity, which means that a large volume fraction of material has been lost preferentially from the disordered interlamellar regions leaving the crystalline component relatively unaffected. Numerous well-developed bands are observed with flat-on lamellae occupying approximately 1/3 the apparent band period

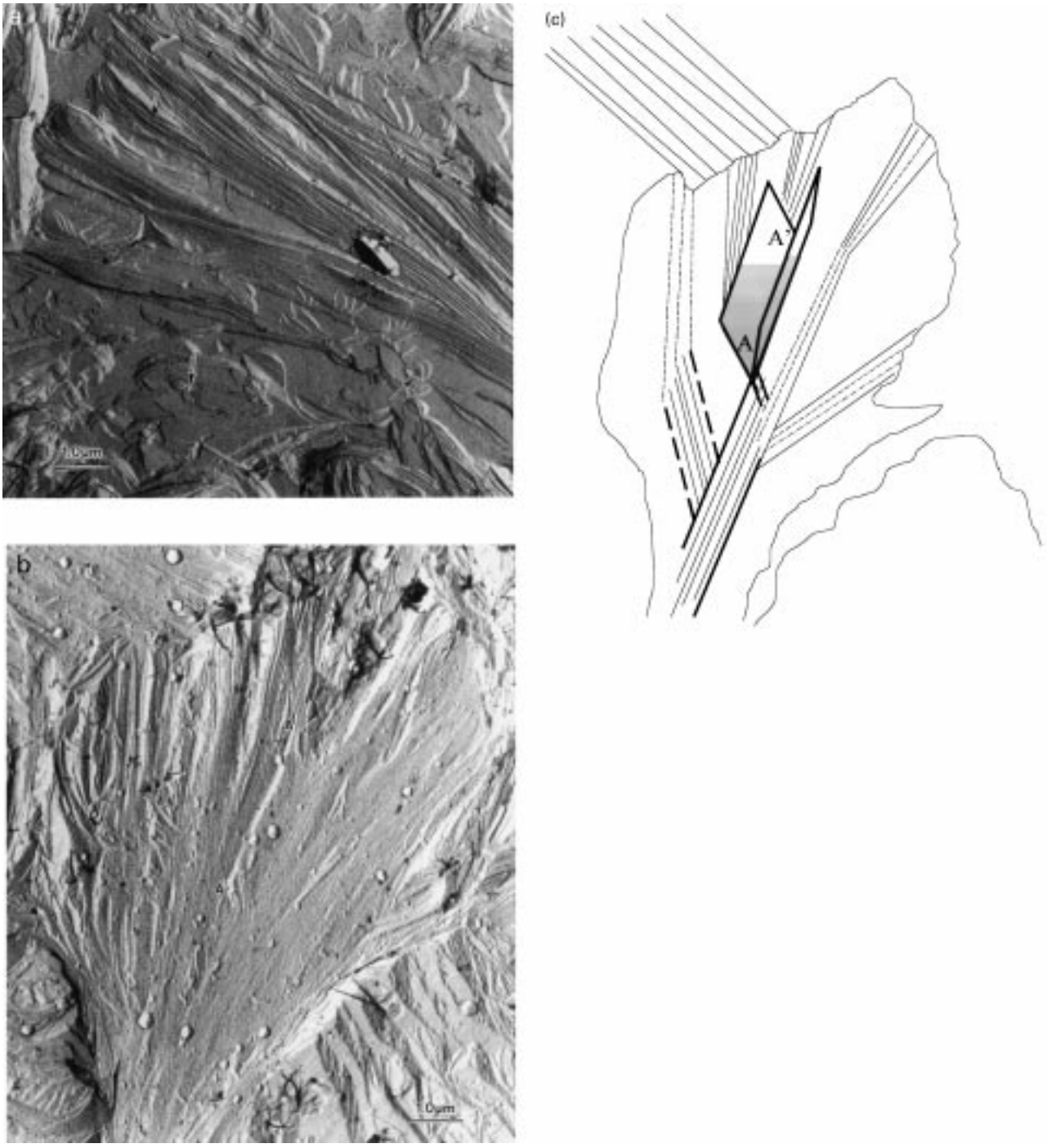

Fig. 4. TEM carbon replica image of etched polymer B showing: (a) crenellated sheaf like features; (b) kink or stacking fault highlighted between space A and A′ shown in the centre of the figure; (c) schematic representation of (b) showing the angular projection of stacking faults that give rise to splay and subsequent branching in immature spherulites.

spacing. The lamellar thickness is essentially unchanged from the previous sample and at the centre of this image there appears to be two points of band initiation; for ease of identification we have labelled these as A and B. Starting from positions A and B and following them around by one-half turn it becomes clear that each consecutive turn reveals a new band. In other words, the banded structure in this polymer appears to be composed of two independent initiation points sharing a common axis of rotation.

Fig. 7 shows an AFM height image of polymer C at large scan size together with a corresponding cross-sectional line profile. The maximum band height (peak-to-trough amplitude) measured on this line profile was approximately 400 nm, as shown by the arrow markers to the right of

Fig. 7. However, if measured on other images not shown here, it varied from 200 to 400 nm. Examining the cross-sectional area reveals an asymmetrical appearance to the banding habit. The leading edge of one lamella is superseded by growth from another lamellar crystal immediately behind it, which leads to the continuous pattern observed. Initially there is a gradual but gentle rise in height associated probably with successive partially twisted lamellae that rotate and extend along **b**.

Fig. 8 shows a TEM image of the highest molecular weight homopolymer (polymer E) with spherulitic domain sizes ranging from a few microns to approximately 7 μm. In this high molecular weight material banding is not observed. We suspect the origins of this lies in the observed enhanced nucleation which curtails the development of spherical symmetry and the occurrence of banding. Instead, S-profiled lamellae are observed with pronounced dominant-subsidiary molecular architectures. Labelled A and B are two particular examples of this type of morphological feature. Note that with increasing molecular weight, the lamellae have become significantly more curved compared with other materials. Generally, the 'ridged' profiles of this in-filling variety (labelled A) are seen surrounded by micron size curved lamellae (labelled B). Interestingly, lamellae that are etched the most are those which are edge-on in contrast to the more etch resistant flat-on lamellae.

Fig. 9 shows the AFM height image of polymer E: (a) large scan size image (low magnification) highlighting specific features that resemble craters; (b) surface topology characterised in terms of spherulite domains. Fig. 9b is identical in magnification to Fig. 8 and both images describe similar morphologies, although the much finer ridge profiled subsidiary lamellae could not be distinguished in the height AFM images, however, they could be detected in the contrast enhanced phase image shown in Fig. 9b. The underlying peak-to-trough amplitude values were approximately 200 nm (line profile) and the lowest recorded within this series of materials. Clearly, the effect of increasing molecular weight reduces the effective etching penetration depth because the lamellae are thicker and are etched over a longer period of time. This slow development in surface relief may also be linked to increased polymer nucleation.

In contrast to all the other materials, Fig. 2c shows the TEM image of polymer D a high-density copolymer. The apparent band spacing was estimated at 2 μm, with flat on lamellae occupying a larger portion of the band period. We estimate this value to be at least 1/4 of the band period spacing. In fact, this copolymer bares a strong resemblance in terms of band structure to another moderately high molecular homopolymer, namely polymer C. In fact, the strong similarities may directly be related to the nature of the catalyst. However, the effects of etching are different with lamellar surfaces exposed edge-on more severely affected than flat-on lamellae. We suspect that short chain branching may influence the way in which rapid surface etching can occur.

Fig. 10 shows the AFM image of Fig. 2c with height contrast showing penetration of etching attaining a maximum depth of approximately 250 nm. However, it should be noted that on other images not shown here, higher values have been measured, up to 350 nm in some cases. Fig. 10a shows the corresponding height image of this sample. Fig. 10b shows a three-dimensional height view of several impinged spherulites. Interestingly the etching depth as indicated by the measurement of height is slightly lower than that previously observed for polymer C of equivalent molecular weight. The etching penetration depth may be related to the affects of short chain branching leading to the observed crystallisation behaviour and spherulitic morphology.

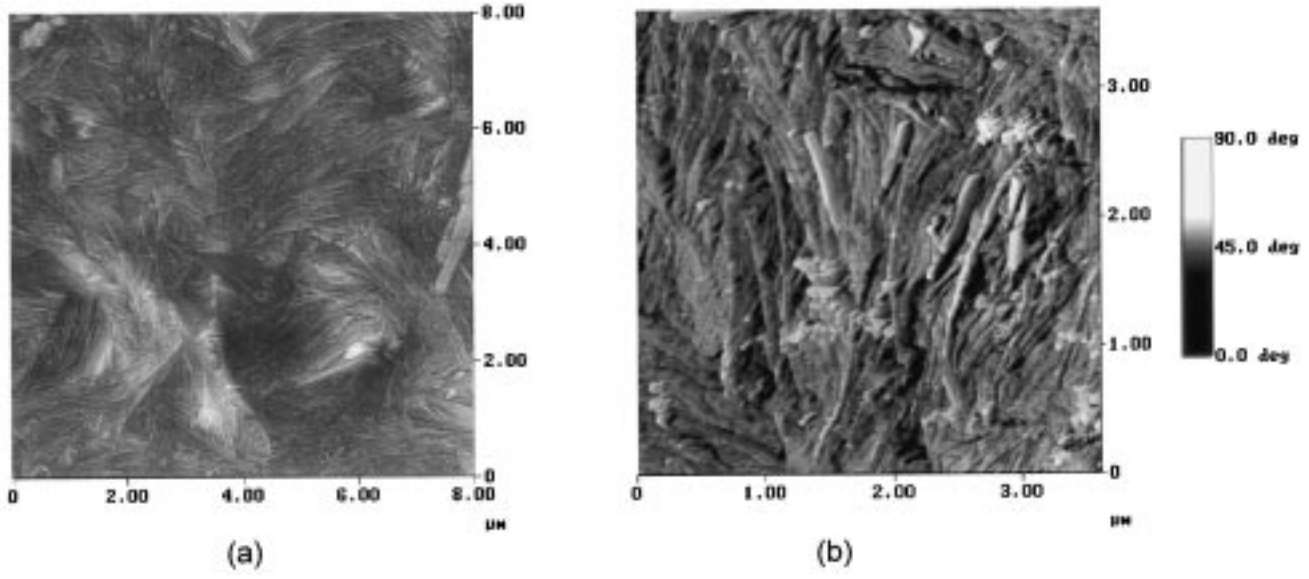

Fig. 5. AFM images of polymer B: (a) contrast enhanced height image; (b) detailed view of twisted lamella in the phase image.

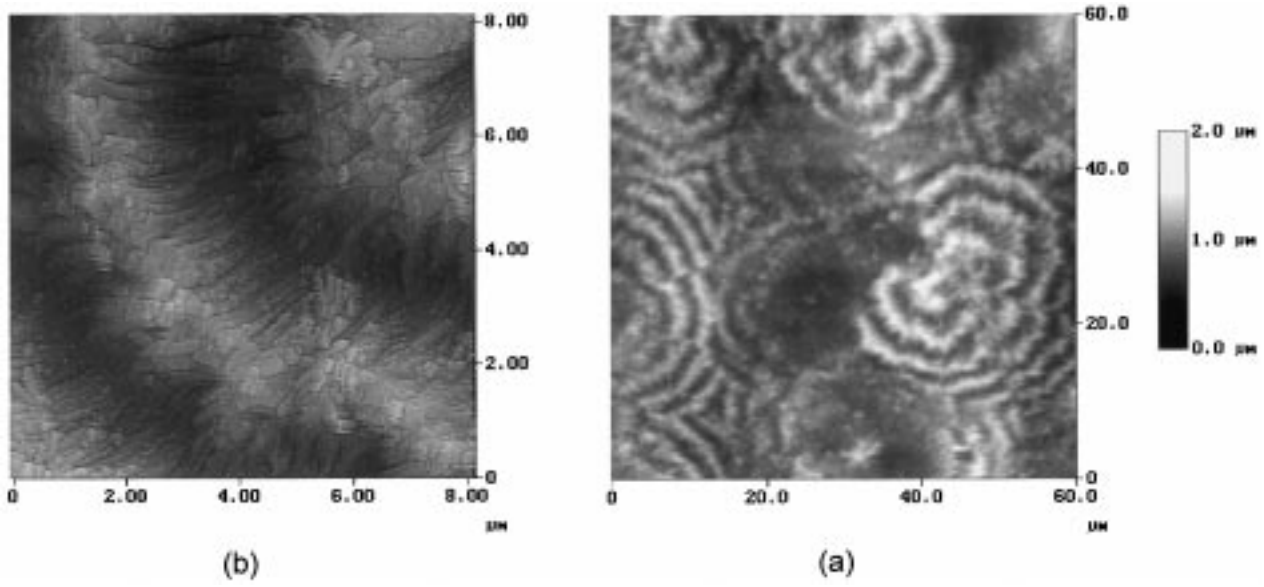

Fig. 6. AFM images of polymer A: (a) large scan size contrast enhanced height image; (b) small scan size contrast enhanced height image.

3.3. Determining the true band spacing

With exception of diametral spherulite sections, in all of the electron micrographs and AFM images presented above we have referred to the apparent band spacing of non-diametral spherulite sections. However, in practice, we can determine the true band spacing for any off-centre section.

Let us consider a model spherulite with a true radial band spacing d and let half-band points sit on the surface of concentric sphere as depicted in Fig. 11. The model spherulite is composed of a series of concentric spheres represented by the following equation:

$$X_i^2 + Y_i^2 + Z_i^2 = r_i^2 \quad (1)$$

with $r_i = i \times d$ where i varies from 1 to the total number of bands. By assuming that microtomy and permanganic etching is equivalent to intersecting a spherulite along a fixed plane of equation $z = a$ (a = constant), the geometric result of this process yields a series of circular discs with variable inter-disc spacing. Fig. 11 illustrates this hypothetical situation, which we believe can account for a large number of observations from TEM and AFM (see above).

$X_{i+1} - X_i$ are apparent band spacing values for the projection of the etched spherulite onto the X–Y plane. It is clear that for a general section the apparent band spacing, $X_{i+1} - X_i$ will decrease with increase in i, converging towards d for large band numbers. In other words, the model predicts that by examining the band period spacings with radial distance it is possible to estimate the correct

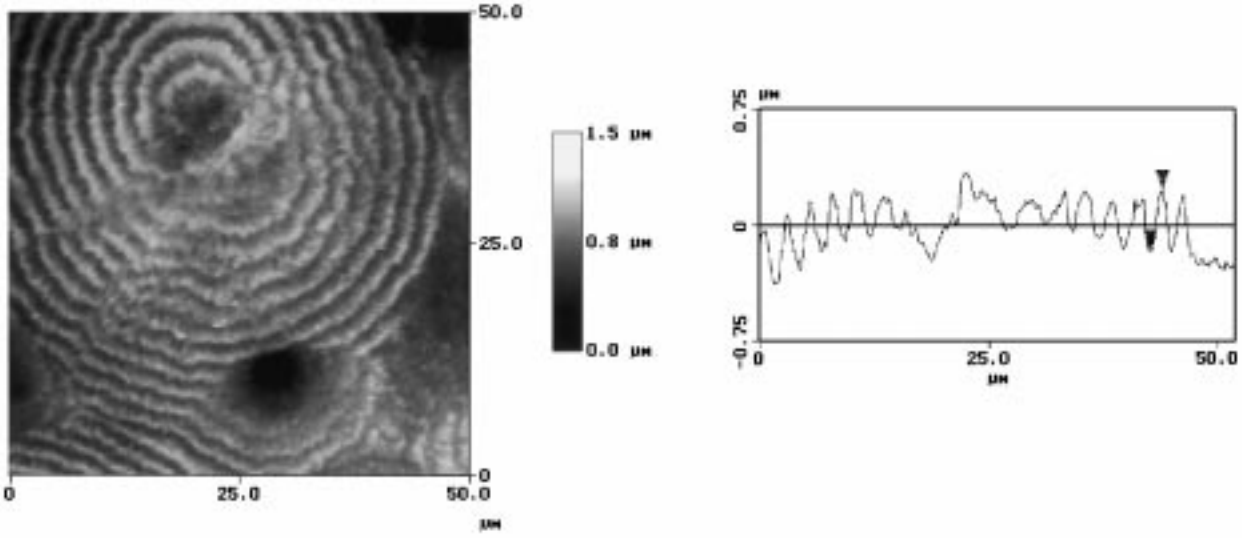

Fig. 7. General overview height image and cross-sectional profile AFM images of polymer C.

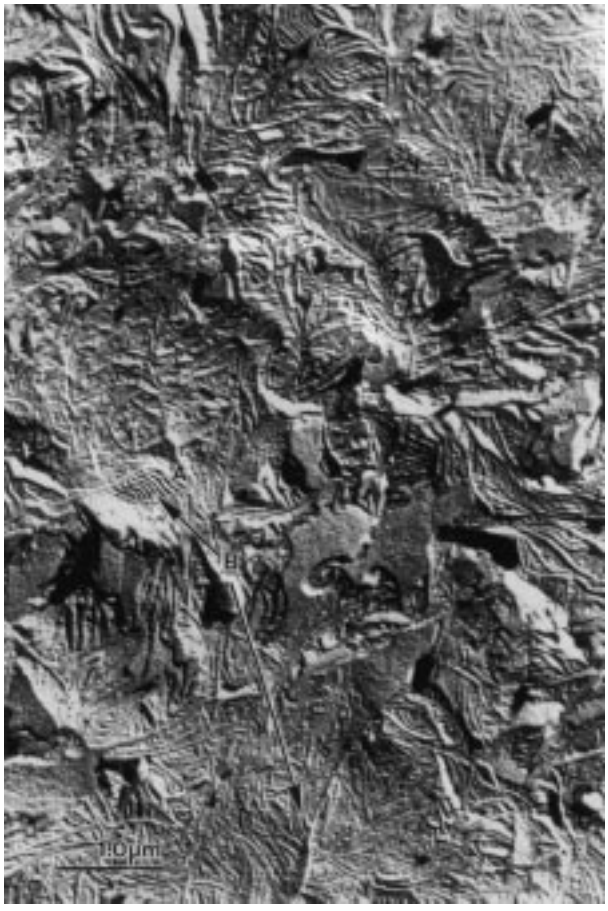

Fig. 8. TEM carbon replica image of etched polymer E. The areas highlighted are given in the text.

band spacing, d. Convergence to d improves with increasing distance away from the nucleus. Eq. (2) describes this relationship analytically, derived from the equation of a series of spheres intersecting a straight line of equation ($z = a,\ y = 0$).

$$X_{i+1} - X_i = d[\sqrt{(i+1)^2 - (a/d)^2} - \sqrt{i^2 - (a/d)^2}] \quad \text{for } i \geq a/d \tag{2}$$

By examining results from AFM and TEM imaging, we attempted to model our data. The spacing between maximum band heights for successive bands was evaluated and compared with the model plot defined by Eq. (2). Fig. 12a–c shows how this relationship is developed with band size for polymers C and D (see Table 1). In the above model, parameters d and a were adjusted manually to the experimental data in order to achieve the best fits. In each case, the experimental data was obtained by averaging several series of $X_{i+1} - X_i$, measured directly from the superposition of several radial lines on a single spherulite. Irrespective of which spherulite is considered d is a constant whereas the a parameter must be adjusted for each spherulite, since it represents the distance between the centre of the spherulite and the etched surface. In the case of polymer C, (Fig. 12a) the best fits were obtained when d was 1.6 μm. In this particular instance, the a parameter was 23 μm for the chosen spherulite. The data were obtained from AFM height images. For polymer D, (Fig. 12b and c) the best fits were achieved when d was 2 μm from AFM measurements and 1.9 μm from TEM measurements. In Fig. 12b, the data from two different spherulites (called A and B) were plotted, resulting in two different fits with the same d but with different values of a ($a = 25.5$ μm for A and 4.8 μm for B).

In Fig. 12c, a was 13 μm. Averaging over several

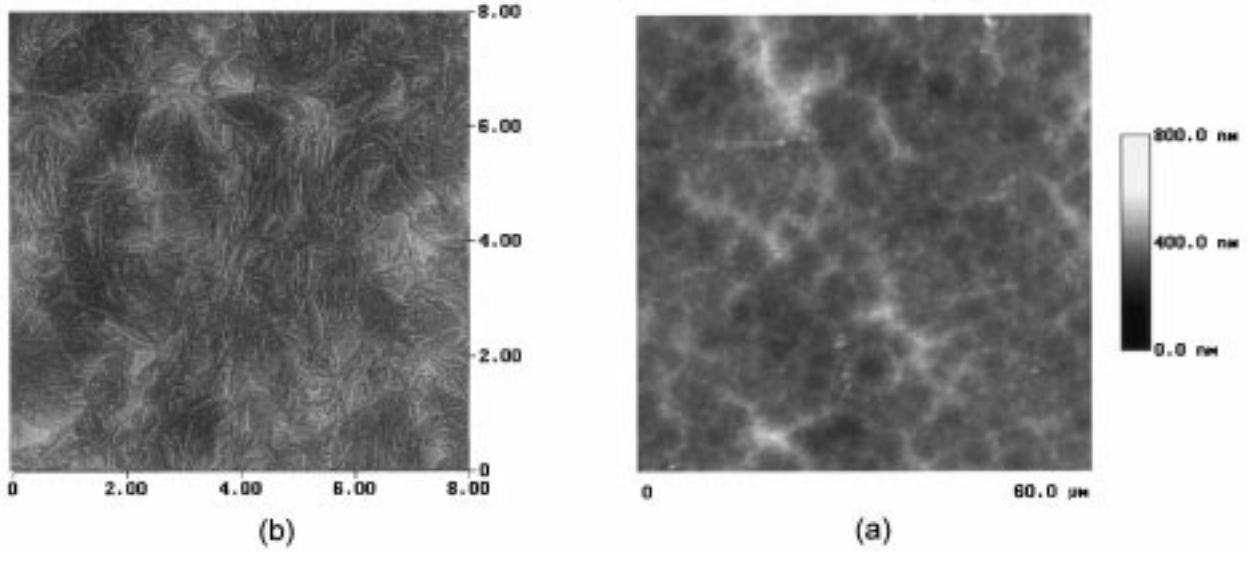

Fig. 9. AFM height images of polymer E: (a) low magnification of impinged spherulitc domain structure; (b) contrast enhanced smaller scan size of (a) depicting characteristic lamellar features.

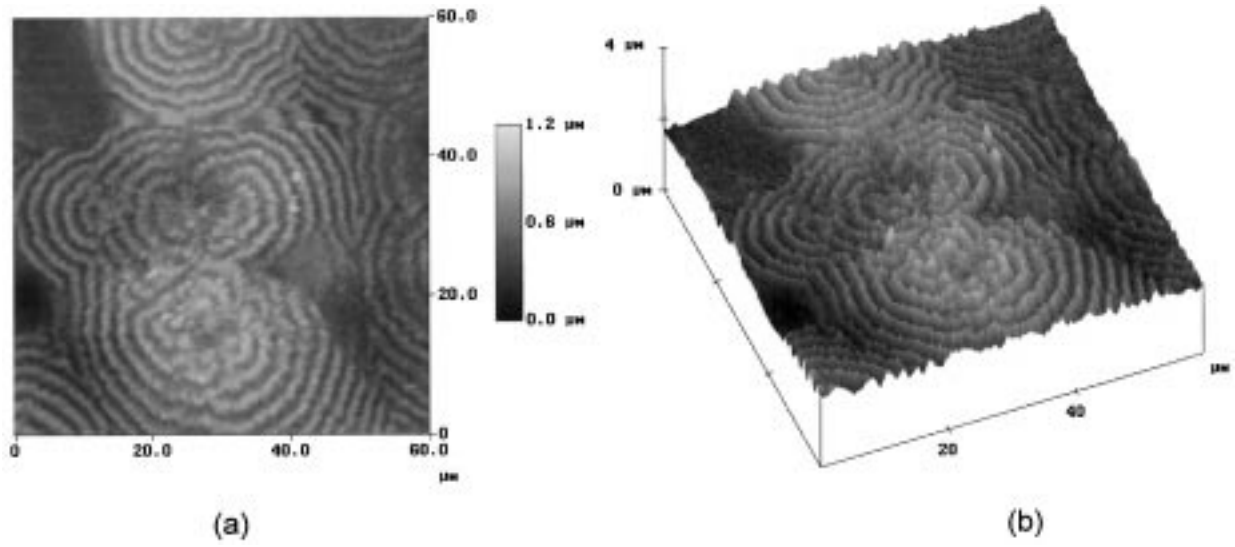

Fig. 10. AFM height images of polymer D: (a) normal height image showing several impinged spherulites; (b) three-dimensional height image at an equivalent scan size.

spherulites of different sizes, we found that the true band spacing from AFM height images lying at the convergence limit of this model were $d \sim 1.6 + /-0.1$ μm and $1.9 + /-0.1$ μm for polymers C and D, respectively. For polymer A, a value of $3.0 + /-0.3$ μm was estimated for d. However we are less confident about the value of this result because of the small number of bands observed in this polymer, making the fit more difficult. It is important to measure apparent band spacings on spherulites exhibiting the greatest number of bands, similarly it is advisable to statistically sample and average over a number of different spherulites, otherwise limited measurements could yield values significantly larger than the true band spacing. In a later paper, we establish a differential-etching model based on the difference in lamellae etching rates between flat-on and edge-on lamellar projections that describes qualitatively the topographic information (profiles) available from AFM height image measurements [31].

4. Conclusions

In metallocene catalysed linear polyethylenes, increasing molecular weight leads progressively to spherulitic geometry via the acknowledged mechanism of lamellar divergence and splay. This leads to the onset of banding that matures into well-defined banded structures for molecular weights above 100,000. For molecular weights less than circa 50,000, the dominant feature is sheaf-like structure. As distinct from copolymers, the true band period becomes smaller while the number of bands increase with increasing molecular weight. Beyond a particular molecular weight range, the banded spherulitc structure is lost and the dominant texture is one of highly nucleated lamellar domains. Little evidence was found to support the view that banding in these mMDPEs arise from collectively twisted lamellar crystals. Moreover, differentiating lamellar curvature from twisting in an individual lamella and lamella curvature

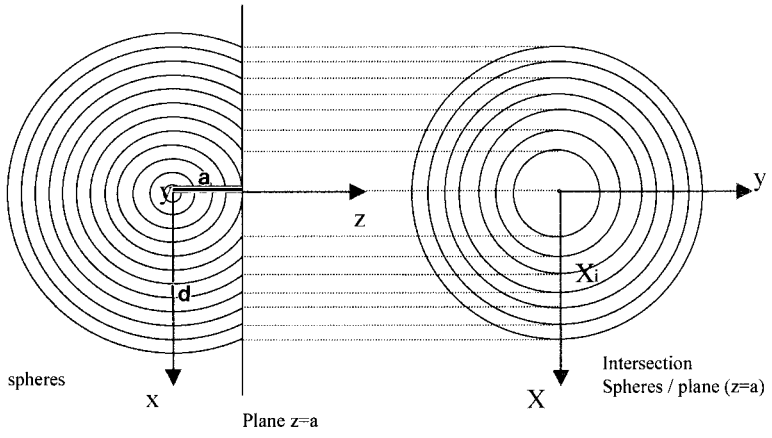

Fig. 11. Modelling of an etched spherulite by a series of concentric spheres sectioned by a plane. Spheres have radii $r_i = i \times d$ where $i = 1$ to n and the constant d is the true band spacing. The $X_{i+1} - X_i$ are the apparent band spacing values for the observed etched spherulite.

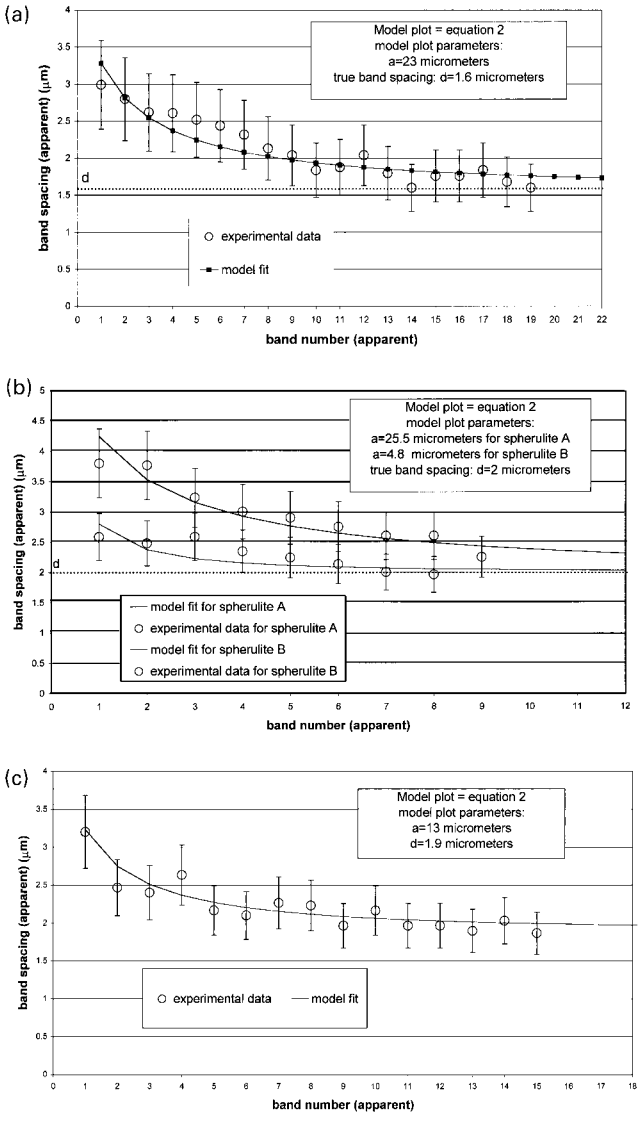

Fig. 12. Model and experimental plot of the apparent band spacing against apparent band number: (a) polymer C from AFM measurements; (b) polymer D from AFM measurements; and (c) polymer D from TEM measurements.

associated with banding en masse becomes harder with increasing molecular weight. Height imaging using AFM offers a direct approach to determining the band period spacing in banded spherulitic systems. Modelling apparent band spacing in non-diametral spherulitic sections as the result of the intersection of a plane with a series of spheres with constant inter-spherical radii reduces the uncertainty in determining the true band spacing. Permanganic etching is sensitive enough to reveal the detailed lamellar structure in mHDPEs. This is linked with exposure penetration depths increasing with decreasing molecular weight which may also be linked to the absence of appreciable interfacial structure.

Acknowledgements

We gratefully acknowledge the support and provision of materials from Fina Research, Feluy (Belgium) and Solvay Polyolefins Europe (Belgium).

References

[1] Keller A. Nature 1952;169:913.
[2] Keller A. J Polym Sci 1955;17:291.
[3] Keller A. J Polym Sci 1959;39:151.
[4] Point J-J. Bull Acad R Belgique 1953;39:435.
[5] Point J-J. Bull Acad R Belgique 1955;41:974 (see also p. 982).
[6] Price FP. J Polym Sci 1959;39:139.
[7] Keith HD, Padden Jr FJ. J Polym Sci 1959;39:101 (see also p. 112).
[8] Bassett DC. Principles of polymer morphology. Cambridge, MA: Cambridge University Press, 1981.
[9] Hedges ES. Lisengang rings and other periodic structures. London: Chapman and Hall, 1932.
[10] George J, Premachandran SK. J Cryst Growth 1979;46:297.
[11] Adamski P, Kazimierski P. J Cryst Growth 1984;66:593.
[12] Bisault J, Ryschenkow G, Faivre G. J Cryst Growth 1991;110:889.
[13] Keller A, Sawada S. Makromol Chem 1964;74:190.
[14] Janimak JJ, Stevens GC. Polymer 2000;41:4223.
[15] Bassett DC. CRC Crit Rev Solid State Mater Sci 1984;12:97.
[16] Lagasse RR. J Cryst Growth 1994;140:370.
[17] Patil R, Reneker DH. Polymer 1994;35:1909.
[18] Hobbs JK, McMaster TJ, Miles MJ, Barham PJ. Polymer 1998;39:2437.
[19] Pearce R, Vancso GJ. J Polym Sci Part B, Polym Phys Ed 1998;36:2643.
[20] Pearce R, Vancso GJ. Polymer 1998;39:1237.
[21] Magonov SN, Reneker DH. Annu Rev Mater Sci 1997;27:175.
[22] Kawai T, Matsumoto T. Makromol Chem 1968;115:287.
[23] Keith HD, Padden Jr FJ. Polymer 1984;25:28.
[24] Proceedings of International Polyethylene Conference. The Institute of Materials, The Connaught Rooms, London, UK, 3–24 October 1997.
[25] Chemistry in Britain. February 1994. p. 87.
[26] Chemistry & industry. November 1994. p. 857.
[27] Kim M-H, Phillips PJ. J Appl Polym Sci 1998;70:1893.
[28] Guo M, Fu Q, Cheng SZD. ACS Polym Preprints 1997;38(2):341.
[29] Freedman AM, Bassett DC, Vaughan AS, Olley RH. Polymer 1986;27:1163.
[30] Bassett DC, Hodge AM. Polymer 1978;19:469.
[31] Markey L, Janimak JJ, Stevens GC. In preparation.